

# Generation of intense terahertz radiation by two-color filamentation of laser pulses with different wavelengths

VLADIMIR YU. FEDOROV<sup>1,2,\*</sup> AND STELIOS TZORTZAKIS<sup>1,3,4,\*\*</sup>

<sup>1</sup>Science Program, Texas A&M University at Qatar, P.O. Box 23874, Doha, Qatar

<sup>2</sup>P. N. Lebedev Physical Institute of the Russian Academy of Sciences, 53 Leninskiy Prospekt, 119991, Moscow, Russia

<sup>3</sup>Institute of Electronic Structure and Laser (IESL), Foundation for Research and Technology - Hellas (FORTH), P.O. Box 1527, GR-71110 Heraklion, Greece

<sup>4</sup>Materials Science and Technology Department, University of Crete, 71003, Heraklion, Greece

\*v.y.fedorov@gmail.com

\*\*stzortz@iesl.forth.gr

**Abstract:** We theoretically study the generation of terahertz (THz) radiation by two-color filamentation of ultrashort laser pulses with different wavelengths. We consider wavelengths in the range from 0.6 to 10.6  $\mu\text{m}$ , thus covering the whole range of existing and future powerful laser sources in the near, mid and far-infrared. We show how different parameters of two-color filaments and generated THz pulses depend on the laser wavelength. We demonstrate that there is an optimal laser wavelength for two-color filamentation that provides the highest THz conversion efficiency and results in generation of extremely intense single cycle THz fields.

© 2018 Optical Society of America under the terms of the [OSA Open Access Publishing Agreement](#)

## 1. Introduction

In the electromagnetic spectrum, the terahertz (THz) frequency range is located in-between the microwave and far-infrared frequencies. For many reasons THz radiation attracts a lot of attention [1, 2]. First, most molecules (especially large biological molecules) have characteristic structural resonances at THz frequencies. Then, the THz part of the electromagnetic spectrum is located at the boundary between spectral ranges characteristic for high frequency electronics and photonics. Therefore, THz devices could play a role of a bridge between these two technologies. Another advantage of THz radiation is its high penetration depth in many materials like plastics, wood, paper, clothings, etc. What is more important, unlike x-rays, THz photons have very low energy and do not ionize matter. As a result, one can use THz radiation in a large number of applications in industrial quality control, medical diagnostics and treatment, homeland security and many others.

Despite the high potential of THz radiation for applications, there is still a huge lack of powerful THz sources. Nowadays, the most powerful table-top sources of THz radiation are based on optical rectification in nonlinear crystals or two-color filamentation [3, 4]. Using optical rectification one can reach 3.7% of THz conversion efficiency (ratio of generated THz energy to energy of input laser pulse) and up to 0.9 mJ of THz pulse energy [5–8]. However the spectrum of the THz pulses generated by optical rectification is quite narrow and limited to frequencies below 5 THz. In turn, with two-color filamentation a typical THz conversion efficiency is lower ( $\sim 0.01\%$ ) and the generated THz pulses are less energetic (up to 30  $\mu\text{J}$  in gases and up to 80  $\mu\text{J}$  in liquids) [9–12]. Nevertheless, compared to optical rectification, THz pulses generated by two-color filamentation are considerably shorter and have much broader spectra ( $>50$  THz). Therefore, in spite of the lower energy, the peak power of such THz pulses can be much higher. Thus, the two-color filamentation technique is a promising tool for generation of THz pulses, powerful enough for studies of nonlinear interactions of THz radiation with matter. Additionally, with two-color filamentation one can generate THz radiation at remote distances, close to the

object of interest, which allows one to overcome strong diffraction of THz fields and their high absorption in atmospheric water vapor [13–16].

Until recently, the majority of experiments on THz generation by two-color filamentation were conducted with Ti:Sapphire laser systems operating at a central wavelength of  $0.8\ \mu\text{m}$ . Nevertheless, an experimental study of two-color filamentation at longer wavelengths showed more than tenfold growth of the THz conversion efficiency when the wavelength of the fundamental laser pulse was increased up to  $1.8\ \mu\text{m}$ , though beyond this wavelength the efficiency dropped down again [17]. The evidence of stronger THz generation at mid-infrared wavelengths was also obtained from Particle in Cell (PIC) simulations of  $4\ \mu\text{m}$  single color laser pulses interacting with gas targets (though without consideration of nonlinear propagation effects) [18].

Recently appeared powerful laser sources, operating at a central wavelength of  $3.9\ \mu\text{m}$  [19], have opened the way to experimental studies of THz generation by laser pulses at the mid-infrared spectral region. In a recent theoretical study, we showed that two-color filamentation of mid-infrared  $3.9\ \mu\text{m}$  laser pulses allows one to generate single cycle THz pulses with multi-millijoule energies and record conversion efficiencies reaching 7% (more than two orders of magnitude higher than for  $0.8\ \mu\text{m}$  laser pulses) [20, 21]. Later, similar results were obtained in [22]. Our recent experiments on two-color filamentation of  $3.9\ \mu\text{m}$  laser pulses [23] confirmed the theoretical predictions. In our theoretical predictions, the focused single cycle THz pulses can reach peak electric and magnetic fields at the GV/cm and kT level respectively. These high conversion efficiencies and field strengths are the result of several factors: stronger photocurrents due to larger ponderomotive forces, negligible walk-off between the fundamental and second harmonic, longer and wider plasma channels, additional field symmetry breaking by generated high harmonics [21].

Despite the above studies there is still an open question about the optimal laser source in terms of its central wavelength for THz generation by two-color filamentation. To answer this question, in this paper we use numerical simulations to study the generation of THz radiation by two-color filamentation of laser pulses with different wavelengths. Our theoretical modeling and simulations have been extensively and successfully benchmarked with experiments at both  $0.8\ \mu\text{m}$  and at  $3.9\ \mu\text{m}$  wavelengths. Here we consider central laser wavelengths in the range from  $0.6$  to  $10.6\ \mu\text{m}$ , thus covering the whole range of existing and future high power laser sources. We show how the parameters of two-color filaments and generated THz pulses depend on the laser wavelength. We demonstrate that for two-color filamentation there is an optimal wavelength of the laser source that provides the highest THz conversion efficiency.

## 2. Model

A detailed description of the model that we use in our simulations can be found in [21]. Briefly, for the simulations of two-color filamentation we use the unidirectional pulse propagation equation (UPPE) coupled with a rate equation for plasma density [24–26]. The UPPE equation is free of slow envelope and paraxial approximations, and has been successfully applied in previous studies of THz generation by near-infrared two-color filaments by many groups beyond ours [27–29]. To precisely describe the dispersion of air refractive index we use the data on absorption lines of oxygen, nitrogen, and carbon dioxide from the HITRAN database [30]. In our simulations we assume that air is dry, thus neglecting the absorption of the generated THz radiation by atmospheric water vapor. Such assumption is justified since we consider only focused laser pulses propagating over short distances. Under these conditions, the whole experimental setup can be placed into a purge gas chamber filled with dry air, as we usually do in our experiments. To calculate the field ionization rate we use the wavelength-dependent Perelomov-Popov-Terent'ev formula [31].

As initial condition for the UPPE equation we use the following two-color field:

$$E = \exp\left(-\frac{r^2}{2a_0^2} - \frac{t^2}{2\tau_0^2}\right)[E_1 \cos(\omega_0 t) + E_2 \cos(2\omega_0 t)], \quad (1)$$

where  $r^2 = x^2 + y^2$ ,  $a_0 = 4/2\sqrt{\ln 2}$  mm is the beam size (4 mm FWHM),  $\tau_0 = 100/2\sqrt{\ln 2}$  fs is the pulse duration (100 fs FWHM),  $\omega_0$  is the central frequency of the fundamental pulse, while  $E_1$  and  $E_2$  being the amplitudes of the fundamental and the second harmonic pulses, respectively. The initial pulse is focused by a lens with the focal distance  $z_f=200$  mm. To simulate the focusing we multiply each Fourier harmonic of the field  $E$  by a factor  $\exp[-i(\omega/c_0)r^2/(2z_f)]$ , where  $\omega$  is the frequency of the corresponding harmonic and  $c_0$  is the speed of light in vacuum.

In our simulations we consider the fundamental pulses with central wavelength  $\lambda_0 = 2\pi c_0/\omega_0$  ranging from 0.6 to 10.6  $\mu\text{m}$ . The energy  $W$  for each wavelength was chosen in such a way that the peak power  $P$  of the corresponding single-color pulse at wavelength  $\lambda_0$  is equal to  $1.2P_{\text{cr}}$ , where  $P_{\text{cr}}$  is the critical power of self-focusing in air at this wavelength. Therefore, since  $P_{\text{cr}} \propto \lambda_0^2$ , the input energy  $W$  also grows quadratically with the wavelength, starting from 0.69 mJ for  $\lambda_0=0.6$   $\mu\text{m}$  and reaching 216 mJ for  $\lambda_0=10.6$   $\mu\text{m}$ . For all wavelengths in our studies the fundamental and second harmonic pulses hold, respectively, 95% and 5% of the input energy  $W$ .

The fixed ratio of peak power to critical power is a fundamental condition for comparing filamentation of laser pulses with different wavelengths. If one would fix the input energy  $W$  of the laser pulses the comparison would be impossible, since at shorter wavelengths one would be in the regime of nonlinear propagation while for far-infrared wavelengths the propagation would be purely linear.

The whole propagation distance in our simulations is equal to 400 mm, which is much shorter than in most previous simulations of mid and far-infrared filamentation, where the propagation distances were tens and hundreds of meters [32–34]. Contrary to filamentation of long-wavelength laser pulses at long distances, where the intensity clamping happens due to shock wave formation rather than by defocusing in plasma [33], for focused long-wavelength laser pulses at short distances plasma becomes the main mechanism of intensity saturation [35].

### 3. Results

In this section we present the results of our simulations of two-color filamentation at different laser wavelengths. In Fig. 1 we show how the peak intensity and peak fluence (integral of the laser pulse intensity over time) vary over distance for laser pulses with different wavelength  $\lambda_0$ . One can see that the maximum peak intensity  $I_{\text{max}}$  is almost independent of the pulse wavelength (see Figs. 1(a) and (c)). However, for longer wavelengths high intensities exist over longer distances (see Fig. 1(a)) which means that laser pulses with longer wavelengths produce longer filaments. In Figs. 1(b) and (d) we see that the maximum value of peak fluence  $F_{\text{max}}$  decreases with the increase of the pulse wavelength. As we will see in the following, such behavior of the peak fluence can be explained by the wider supercontinuum spectrum for laser pulses with longer wavelength and, as a result, more effective pulse shortening during filamentation (we remind that fluence is the integral of the laser pulse intensity over time).

Figure 2 shows the dependence of the filament length (calculated as the FWHM length of the fluence distribution along  $z$ ) and filament diameter (calculated as the minimal along  $z$  FWHM diameter of the fluence distribution) on the wavelength  $\lambda_0$  of the fundamental pulse. We see that both the length and diameter of the filament increase as a function of the pump wavelength. Thus, for laser pulses with longer wavelength the filaments are not only longer but also thicker. As expected, the same observation is true for the corresponding plasma channels: they also become longer and thicker with increase of  $\lambda_0$ .

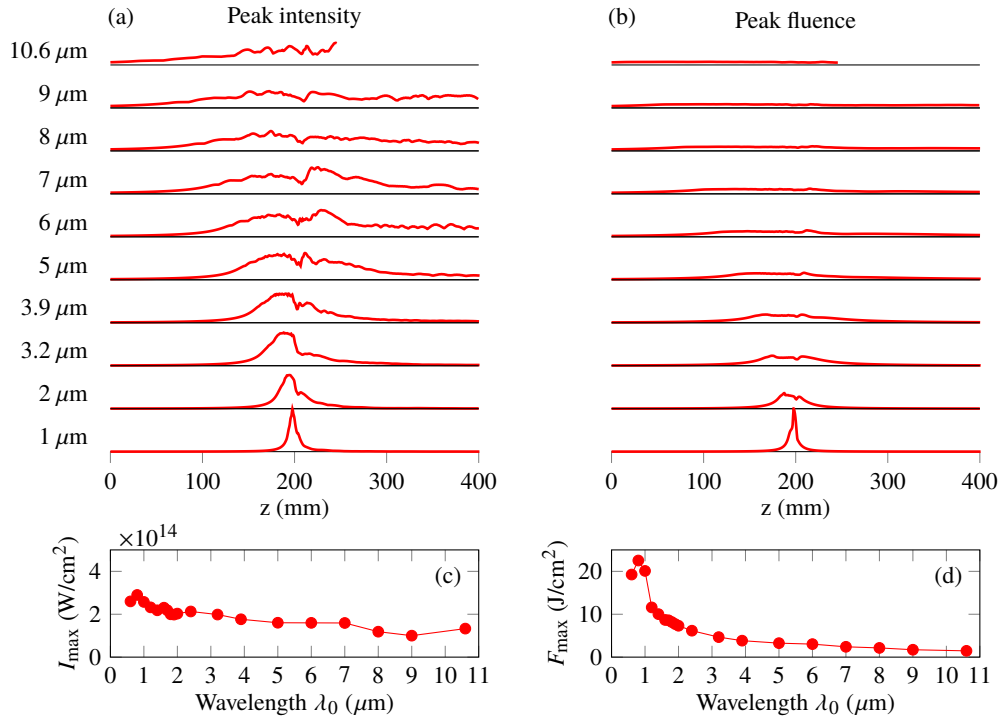


Fig. 1. (a) Normalized peak intensity and (b) peak fluence versus propagation distance for several wavelengths  $\lambda_0$  of the fundamental pulse. The normalization factor is the same for all wavelengths. (c) Maximum peak intensity  $I_{\text{max}}$  and (d) maximum peak fluence  $F_{\text{max}}$  versus the wavelength  $\lambda_0$  of the fundamental pulse.

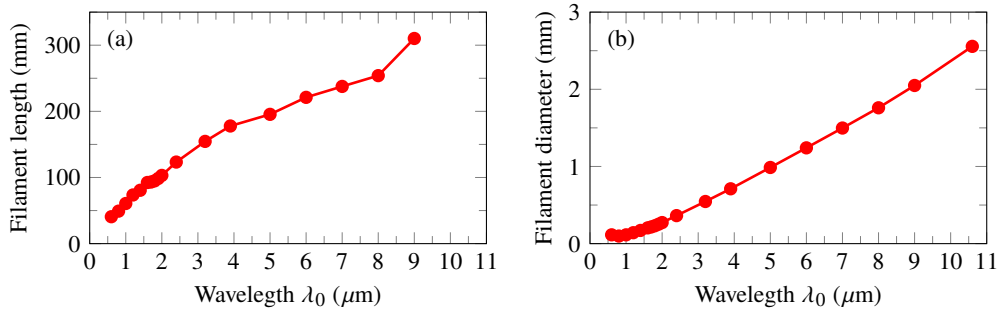


Fig. 2. (a) Filament length (FWHM) and (b) filament diameter (FWHM) versus the wavelength  $\lambda_0$  of the fundamental pulse.

Figure 3 shows the dependence of peak and integrated (over radius) plasma densities on propagation distance for laser pulses with different wavelength  $\lambda_0$ . In Figs. 3(a) and (c) we see that the maximum peak plasma density  $\rho_{\max}$ , being high for near infrared pulses, starting from approximately  $\lambda_0=1 \mu\text{m}$ , drops down. Then, for mid and far-infrared pulses,  $\rho_{\max}$  increases again and reaches similar values to the ones for near-infrared pulses. This transition can be explained by the interplay between the field and avalanche ionizations, since the avalanche ionization becomes more important at longer wavelengths. For near infrared and shorter wavelengths most of the plasma free electrons are produced by the field ionization. With increase of the wavelength, the probability of the field ionization drops down and we start to see less plasma density. However, the ponderomotive forces exerted by mid and far-infrared laser pulses become strong enough to effectively accelerate free electrons, which results in enhanced avalanche ionization and generation of more plasma. This behavior is confirmed by our simulations, where we see almost no plasma generation for mid and far-infrared pulses when we switch-off the avalanche ionization.

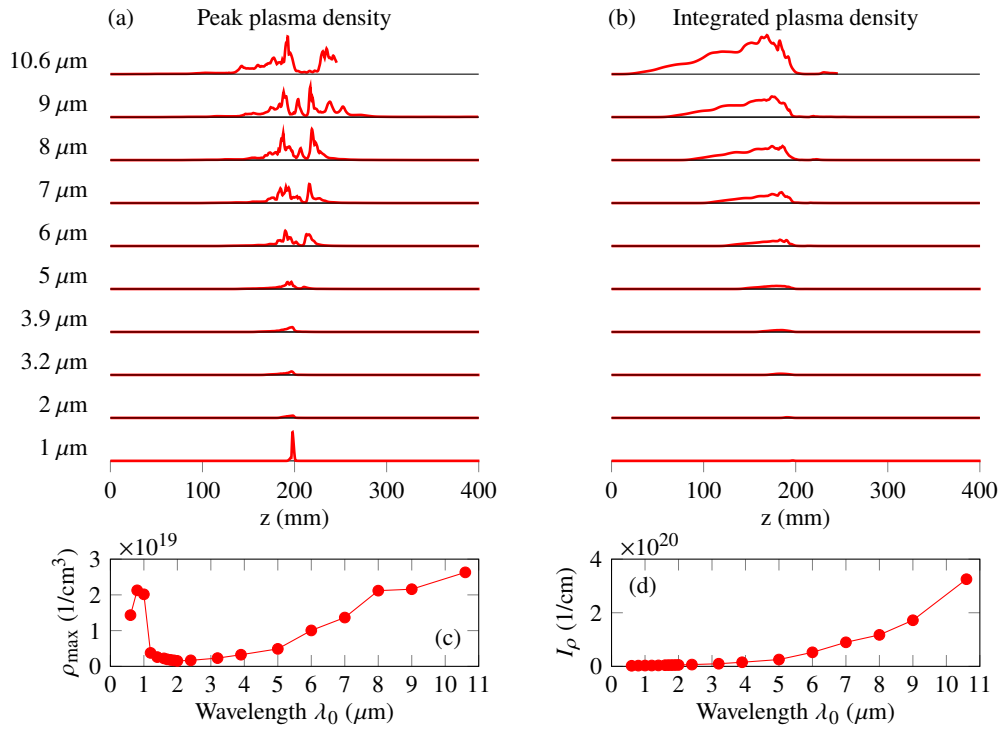


Fig. 3. Normalized peak (a) and integrated over radius (b) plasma densities versus propagation distance for several wavelengths  $\lambda_0$  of the fundamental pulse. The normalization factor is the same for all wavelengths. (c) Maximum peak plasma density  $\rho_{\max}$  and (d) maximum integrated plasma density  $I_\rho$  versus the wavelength  $\lambda_0$  of the fundamental pulse.

Figure 3(d) shows that the maximum value of the integrated plasma density,  $I_\rho$ , monotonically increases with increase of the pulse central wavelength  $\lambda_0$ . Taking into account that the peak plasma densities for far and near infrared pulses are close (see Fig. 3(c)), we conclude that this increase of  $I_\rho$  happens because plasma channels, produced by laser pulses with higher  $\lambda_0$ , are wider (see Fig. 2). From Fig. 3(b) we can also conclude that for higher  $\lambda_0$  the plasma channels are longer. For example, for  $\lambda_0=10.6 \mu\text{m}$  the plasma channel is being formed almost immediately after the laser pulse starts to propagate in the atmosphere. The ponderomotive forces for such long-wavelength laser pulses are so strong that even a small seed of free electrons produced by field ionization is enough to generate a huge amount of secondary free electrons through

avalanche ionization. To sum up, due to longer and wider plasma channels, the total amount of free electrons produced by laser pulses with longer wavelength increases.

In Fig. 4 we show the dependence of the integrated (over radius) power spectrum on the propagation distance  $z$  and frequency  $f$  for laser pulses with central wavelength 3.2, 6, and 9  $\mu\text{m}$ . For all three wavelengths  $\lambda_0$  we see the formation of multiple higher harmonics. However, while for  $\lambda_0=3.2 \mu\text{m}$  all higher harmonics remain spectrally separated over the whole propagation distance, for  $\lambda_0=6$  and 9  $\mu\text{m}$ , after plasma formation, the higher harmonics merge together and form uninterrupted supercontinua, extending down to the ultraviolet absorption band of the atmosphere. This merging of higher harmonics happens, because the distance between the neighboring harmonics is inversely proportional to  $\lambda_0$ . As a result, in case of long-wavelength laser pulses, spectral broadening and blue shifting in plasma fill the gaps between the harmonics much easier. As we have shown in our previous study [21], the various harmonic pairs play a significant role in enhancing the plasma photocurrents and consequently the THz conversion efficiency.

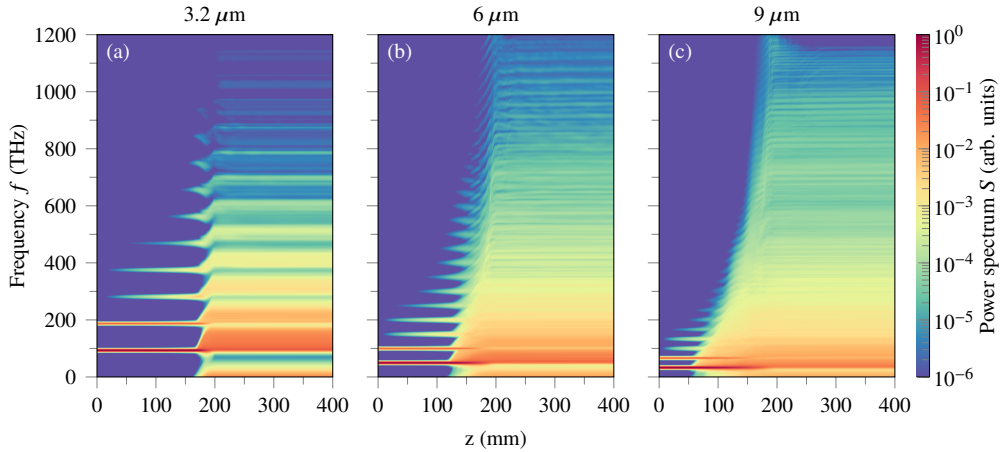


Fig. 4. Dependence of the integrated over radius pulse power spectrum  $S$  on the propagation distance  $z$  and frequency  $f$  for (a) 3.2  $\mu\text{m}$ , (b) 6  $\mu\text{m}$ , and (c) 9  $\mu\text{m}$  two-color laser pulses.

Figure 5 shows the integrated (over radius) power spectra, obtained at a distance of 200 mm (lens focus), for two-color laser pulses with different wavelengths  $\lambda_0$ . Here again we see that for near and mid-infrared laser pulses we can distinguish separate higher harmonics generated during nonlinear propagation. However, for far-infrared laser pulses all harmonics merge together and form uninterrupted supercontinuum spectra that cover the whole range from the THz up to ultraviolet frequencies. This effect also explains the decreasing peak fluence observed in Fig. 1(d).

In Fig. 5 we also see that for all wavelengths  $\lambda_0$  a considerable part of the laser pulse energy transfers to THz frequencies. However, it is not so straightforward to separate the generated THz radiation from the rest of the spectrum, especially in the case of far-infrared pulses. For example, for laser pulses with  $\lambda_0=10.6 \mu\text{m}$ , the central frequency  $f_0 = \omega_0/2\pi$  is equal to 28 THz, so the fundamental pulse itself can be called a THz pulse. In order to give a common definition of the generated THz pulse, independently of the laser pulse wavelength, we define the generated THz radiation as all frequencies that lie below half of the laser central frequency, that is, below  $f_0/2$ . For each wavelength  $\lambda_0$  in Fig. 5 the gray shaded area shows the part of the laser pulse spectrum that, according to our definition, corresponds to the generated THz pulse. As one can see, the spectrum of the generated THz pulses narrows down with increase of  $\lambda_0$ .

In principle, one could define the generated THz radiation as radiation with frequencies

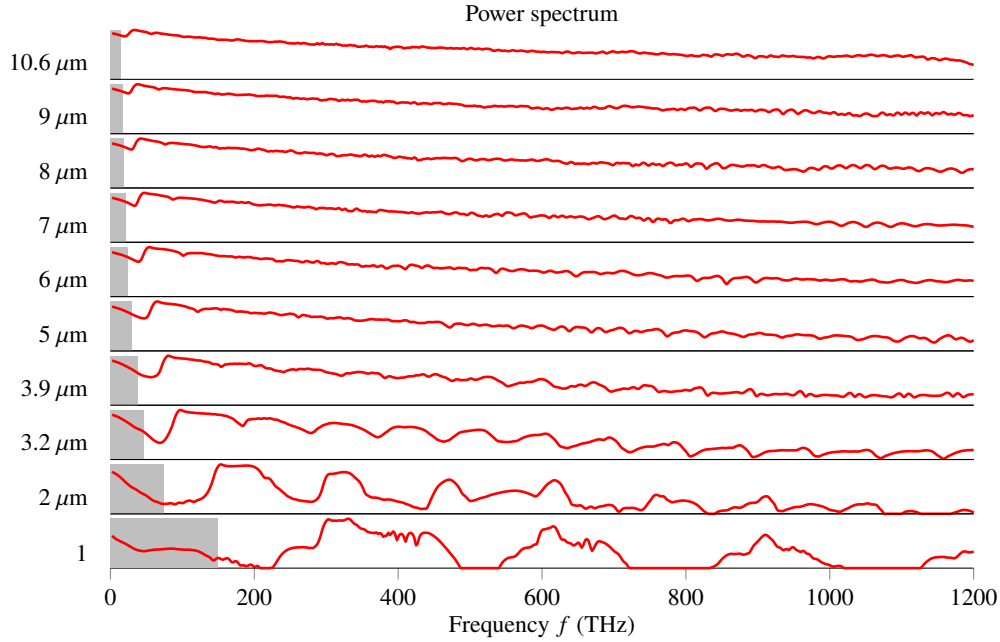


Fig. 5. Normalized power spectra (integrated over radius) of laser pulses with different wavelength  $\lambda_0$ . The plots are in log scale and the normalization factor is the same for all wavelengths. All spectra are obtained in the point of lens focus at distance 200 mm.

below some fixed frequency, e.g. 15 THz. However, such definition, being applied for near and mid-infrared pulses, would exclude all higher THz frequencies that are generated during two-color filamentation. In other words, such definition would neglect the fact that two-color filamentation is a source of ultra-broadband THz radiation.

Figure 6 shows how different parameters of the generated THz pulses depend on the wavelength  $\lambda_0$  of the two-color laser source. In Fig. 6(a) we see the dependence of energy of the generated THz pulses  $W_{\text{THz}}$  on  $\lambda_0$ . Since in our simulations we fix the  $P/P_{\text{cr}}$  ratio and  $P_{\text{cr}} \propto \lambda_0^2$ , the input laser energy is also proportional to the square of  $\lambda_0$ . Therefore, in order to have the same or growing THz conversion efficiency while increasing the laser wavelength,  $W_{\text{THz}}$  should increase at least as  $\lambda_0^2$ . However, according to Fig. 6(a) the THz energy grows non-monotonically with wavelength  $\lambda_0$ . As a result, the THz conversion efficiency  $Q_{\text{THz}}$  depends on  $\lambda_0$  in a peculiar way (see Fig. 6(b)): First,  $Q_{\text{THz}}$  rapidly grows while  $\lambda_0$  increases up to approximately 1.6  $\mu\text{m}$ , but then drops down, reaching its minimum near  $\lambda_0=1.8 \mu\text{m}$ . This part of the  $Q_{\text{THz}}$  dependence is very similar to the experimental observations in [17]. After 1.8  $\mu\text{m}$ , THz conversion efficiency starts to grow again and reaches its maximum value of about 7% around  $\lambda_0=3.2 \mu\text{m}$ . Then, at longer wavelengths  $Q_{\text{THz}}$  monotonically decreases. Since the THz conversion efficiency has a global maximum near  $\lambda_0=3.2 \mu\text{m}$ , we can conclude that this laser wavelength is the optimal one for all THz sources based on two-color filamentation.

Here we should stress the importance of the propagation effects. According to the photocurrent model [36], that is usually used to explain the mechanism of THz generation by two-color filamentation, THz energy should continuously grow with increase of the laser wavelength  $\lambda_0$ . Thus, the peculiar dependence of THz energy on  $\lambda_0$  is the result of the complex interplay between linear and nonlinear effects during the laser pulse propagation.

Figure 6(c) shows the dependence of the peak THz electric field  $E_{\text{THz}}$  on the wavelength  $\lambda_0$  of the two-color laser source. We see that for mid and far-infrared laser pulses  $E_{\text{THz}}$  is higher

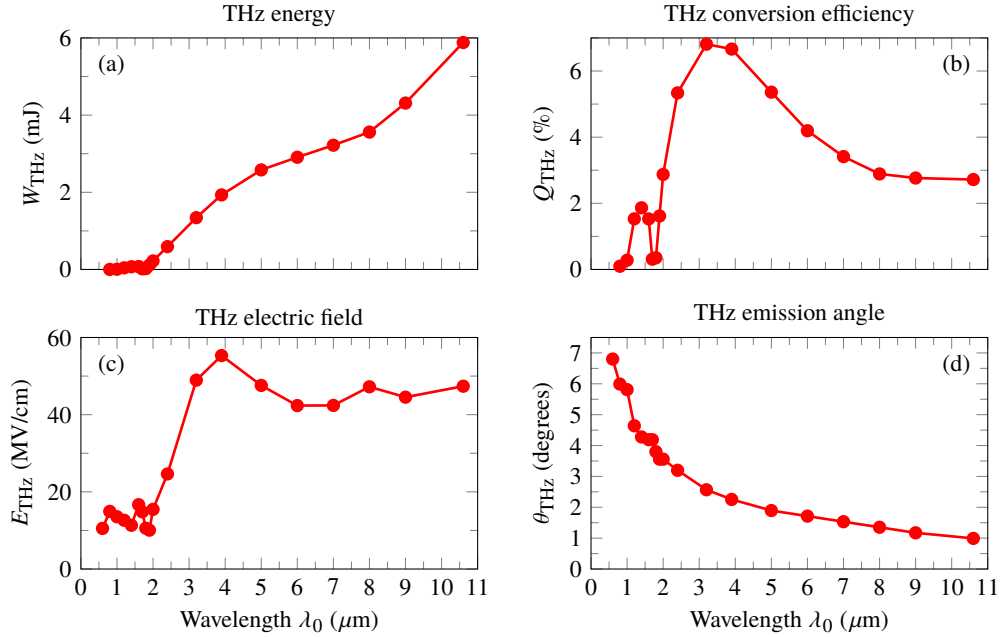


Fig. 6. (a) Energy of generated THz pulse  $W_{\text{THz}}$ , (b) THz conversion efficiency  $Q_{\text{THz}}$ , (c) peak THz electric field  $E_{\text{THz}}$ , and (d) THz emission angle  $\theta_{\text{THz}}$  versus the wavelength  $\lambda_0$  of the fundamental laser pulse.

than for near-infrared ones. Though, starting from  $\lambda_0 \approx 3 \mu\text{m}$  the peak THz electric field is almost independent of  $\lambda_0$  and approximately equal to 50 MV/cm. Note that this field strength corresponds to THz pulses inside the filamentation zone. By collecting the THz radiation and refocusing it after the filament, using for example simple parabolic mirrors, one can reach significantly higher electric and magnetic THz fields of GV/cm and kT level [21].

In the spatial domain the THz radiation generated by two-color filamentation is emitted into a cone [37–40]. Figure 6(d) shows a monotonic decrease of the angle  $\theta_{\text{THz}}$  of this THz cone as a function of increasing laser wavelength  $\lambda_0$ . This effect is linked to the longer and thicker filament plasma channels (see Fig. 2) at longer pump wavelengths as explained by the interference model [40]. Thus, the THz radiation generated by laser pulses with longer wavelengths is better directed.

#### 4. Conclusion

In conclusion, we used numerical simulations to study the generation of THz radiation by two-color filamentation of laser pulses with different wavelength. We considered laser wavelengths in the range from 0.6 to 10.6  $\mu\text{m}$ . This spectral range includes all existing and future high power ultrashort laser sources. We have shown that laser pulses with longer wavelengths produce longer and wider filaments and plasma channels. The total amount of free electrons produced by laser pulses increases with increasing laser wavelength. Also, we demonstrated that two-color filamentation of far-infrared laser pulses is accompanied by the formation of extremely broad uninterrupted supercontinua that extend from THz up to ultraviolet frequencies. We have shown that using mid and far-infrared two-color laser pulses one can generate THz laser pulses whose electric fields are about 50–60 MV/cm inside the filamentation zone and can exceed the GV/cm level through further focusing. Also we demonstrated that the THz radiation for laser pulses with longer wavelengths is better directed: the angle of the THz conical emission reduces with



increase of the laser wavelength. Moreover, we have shown that the highest THz conversion efficiency of  $\approx 7\%$  is reached for two-color laser sources operating at wavelengths close to  $3.2 \mu\text{m}$ . Thus, we found the optimal laser wavelength for THz generation by two-color filamentation, which opens the way to extreme nonlinear THz science.

## Funding

This work was supported by the National Priorities Research Program grant No. NPRP9-329-1-067 from the Qatar National Research Fund (member of The Qatar Foundation), the H2020 Laserlab-Europe (EC-GA 654148), and the H2020 MIR-BOSE (EC-GA 737017).

## References

1. X. C. Zhang, A. Shkurinov, and Y. Zhang, "Extreme terahertz science," *Nat. Photonics* **11**, 16–18 (2017).
2. M. Tonouchi, "Cutting-edge terahertz technology," *Nat. Photonics* **1**, 97–105 (2007).
3. R. A. Lewis, "A review of terahertz sources," *J. Phys. D: Appl. Phys.* **47**, 374001 (2014).
4. K. Reimann, "Table-top sources of ultrashort THz pulses," *Reports on Prog. Phys.* **70**, 1597–1632 (2007).
5. W. R. Huang, S.-W. Huang, E. Granados, K. Ravi, K.-H. Hong, L. E. Zapata, and F. X. Kärtner, "Highly efficient terahertz pulse generation by optical rectification in stoichiometric and cryo-cooled congruent lithium niobate," *J. Mod. Opt.* **62**, 1–8 (2014).
6. C. Vicario, A. V. Ovchinnikov, S. I. Ashitkov, M. B. Agranat, V. E. Fortov, and C. P. Hauri, "Generation of 0.9-mJ THz pulses in DSTMS pumped by a Cr:Mg<sub>2</sub>SiO<sub>4</sub> laser," *Opt. Lett.* **39**, 6632–6635 (2014).
7. J. A. Fülöp, Z. Ollmann, C. Lombosi, C. Skrobol, S. Klingebiel, L. Pálfalvi, F. Krausz, S. Karsch, and J. Hebling, "Efficient generation of THz pulses with 0.4 mJ energy," *Opt. Express* **22**, 20155 (2014).
8. M. Shalaby and C. P. Hauri, "Demonstration of a low-frequency three-dimensional terahertz bullet with extreme brightness," *Nat. Commun.* **6**, 1–8 (2015).
9. K. Y. Kim, A. J. Taylor, J. H. Glowina, and G. Rodriguez, "Coherent control of terahertz supercontinuum generation in ultrafast laser-gas interactions," *Nat. Photonics* **2**, 605–609 (2008).
10. T. I. Oh, Y. J. Yoo, Y. S. You, and K. Y. Kim, "Generation of strong terahertz fields exceeding 8 MV/cm at 1 kHz and real-time beam profiling," *Appl. Phys. Lett.* **105**, 041103 (2014).
11. D. Kuk, Y. J. Yoo, E. W. Rosenthal, N. Jhaji, H. M. Milchberg, and K. Y. Kim, "Generation of scalable terahertz radiation from cylindrically focused two-color laser pulses in air," *Appl. Phys. Lett.* **108**, 121106 (2016).
12. I. Dey, K. Jana, V. Y. Fedorov, A. D. Koulouklidis, A. Mondal, M. Shaikh, D. Sarkar, A. D. Lad, S. Tzortzakis, A. Couairon, and G. R. Kumar, "Highly efficient broadband terahertz generation from ultrashort laser filamentation in liquids," *Nat. Commun.* **8**, 1184 (2017).
13. T. J. Wang, S. Yuan, Y. Chen, J. F. Daigle, C. Marceau, F. Théberge, M. Châteauneuf, J. Dubois, and S. L. Chin, "Toward remote high energy terahertz generation," *Appl. Phys. Lett.* **97**, 111108 (2010).
14. T. J. Wang, J. F. Daigle, S. Yuan, F. Théberge, M. Châteauneuf, J. Dubois, G. Roy, H. Zeng, and S. L. Chin, "Remote generation of high-energy terahertz pulses from two-color femtosecond laser filamentation in air," *Phys. Rev. A* **83**, 053801 (2011).
15. J.-F. Daigle, F. Théberge, M. Henriksson, T.-J. J. Wang, S. Yuan, M. Châteauneuf, J. Dubois, M. Piché, and S. L. Chin, "Remote THz generation from two-color filamentation: long distance dependence," *Opt. Express* **20**, 6825–6834 (2012).
16. K. Liu, A. D. Koulouklidis, D. G. Papazoglou, S. Tzortzakis, and X.-C. Zhang, "Enhanced terahertz wave emission from air-plasma tailored by abruptly autofocusing laser beams," *Optica* **3**, 605–608 (2016).
17. M. Clerici, M. Peccianti, B. E. Schmidt, L. Caspani, M. Shalaby, M. Giguère, A. Lotti, A. Couairon, F. Légaré, T. Ozaki, D. Faccio, and R. Morandotti, "Wavelength scaling of terahertz generation by gas ionization," *Phys. Rev. Lett.* **110**, 253901 (2013).
18. W.-M. Wang, S. Kawata, Z.-M. Sheng, Y.-T. Li, L.-M. Chen, L.-J. Qian, and J. Zhang, "Efficient terahertz emission by mid-infrared laser pulses from gas targets," *Opt. Lett.* **36**, 2608–2610 (2011).
19. A. V. Mitrofanov, A. A. Voronin, D. A. Sidorov-Biryukov, A. Pugžlys, E. A. Stepanov, G. Andriukaitis, T. Flöry, S. Ališauskas, A. B. Fedotov, A. Baltuška, and A. M. Zheltikov, "Mid-infrared laser filaments in the atmosphere," *Sci. Reports* **5**, 8368 (2015).
20. V. Y. Fedorov and S. Tzortzakis, "Extreme THz fields from two-color filamentation of mid-infrared laser pulses," *arXiv:1708.07310* (2017).
21. V. Y. Fedorov and S. Tzortzakis, "Extreme THz fields from two-color filamentation of midinfrared laser pulses," *Phys. Rev. A* **97**, 063842 (2018).
22. A. Nguyen, P. González de Alaiza Martínez, I. Thiele, S. Skupin, and L. Bergé, "Broadband terahertz radiation from two-color mid- and far-infrared laser filaments in air," *Phys. Rev. A* **97**, 063839 (2018).
23. A. D. Koulouklidis, C. Gollner, V. Shumakova, V. Y. Fedorov, A. Pugžlys, A. Baltuška, and S. Tzortzakis, "Strong thz fields from mid-infrared two-color laser filaments," in *Book of abstracts of International Conference on Laser Filamentation (COFIL)*, (2018), pp. 54–55.

24. M. Kolesik, J. V. Moloney, and M. Mlejnek, "Unidirectional Optical Pulse Propagation Equation," *Phys. Rev. Lett.* **89**, 283902 (2002).
25. M. Kolesik and J. V. Moloney, "Nonlinear optical pulse propagation simulation: From Maxwell's to unidirectional equations," *Phys. Rev. E* **70**, 036604 (2004).
26. A. Couairon, E. Brambilla, T. Corti, D. Majus, O. Ramírez-Góngora, and M. Kolesik, "Practitioner's guide to laser pulse propagation models and simulation," *The Eur. Phys. J. Special Top.* **199**, 5–76 (2011).
27. I. Babushkin, W. Kuehn, C. Köhler, S. Skupin, L. Bergé, K. Reimann, M. Woerner, J. Herrmann, and T. Elsaesser, "Ultrafast Spatiotemporal Dynamics of Terahertz Generation by Ionizing Two-Color Femtosecond Pulses in Gases," *Phys. Rev. Lett.* **105**, 053903 (2010).
28. L. Bergé, S. Skupin, C. Köhler, I. Babushkin, and J. Herrmann, "3D numerical simulations of THz generation by two-color laser filaments," *Phys. Rev. Lett.* **110**, 073901 (2013).
29. V. A. Andreeva, O. G. Kosareva, N. A. Panov, D. E. Shipilo, P. M. Solyankin, M. N. Esaulkov, P. G. D. A. Martínez, A. P. Shkurinov, V. A. Makarov, L. Bergé, and S. L. Chin, "Ultrabroad Terahertz Spectrum Generation from an Air-Based Filament Plasma," *Phys. Rev. Lett.* **116**, 063902 (2016).
30. "HITRAN on the Web," <http://hitran.iao.ru/>.
31. A. M. Perelomov, V. S. Popov, and M. V. Terent'ev, "Ionization of atoms in an alternating electric field: II," *Sov. Phys. JETP* **24**, 207–217 (1967).
32. Y. E. Geints and A. A. Zemlyanov, "Dynamics of CO<sub>2</sub> laser pulse filamentation in air influenced by spectrally selective molecular absorption," *Appl. Opt.* **53**, 5641–5648 (2014).
33. P. Panagiotopoulos, P. Whalen, M. Kolesik, and J. V. Moloney, "Super high power mid-infrared femtosecond light bullet," *Nat. Photonics* **9**, 543–548 (2015).
34. N. A. Panov, D. E. Shipilo, V. A. Andreeva, O. G. Kosareva, A. M. Saletsky, H. Xu, and P. Polynkin, "Supercontinuum of a 3.9- $\mu\text{m}$  filament in air: Formation of a two-octave plateau and nonlinearly enhanced linear absorption," *Phys. Rev. A* **94**, 041801 (2016).
35. V. Shumakova, S. Ališauskas, P. Malevich, C. Gollner, A. Baltuška, D. Kartashov, A. M. Zheltikov, A. V. Mitrofanov, A. A. Voronin, D. A. Sidorov-Biryukov, and A. Pugžlys, "Filamentation of Mid-IR pulses in ambient air in the vicinity of molecular resonances," *Opt. Lett.* **43**, 2185–2188 (2018).
36. K.-Y. Kim, J. H. Glowina, A. J. Taylor, and G. Rodríguez, "Terahertz emission from ultrafast ionizing air in symmetry-broken laser fields," *Opt. Express* **15**, 4577–4584 (2007).
37. H. Zhong, N. Karpowicz, and X. C. Zhang, "Terahertz emission profile from laser-induced air plasma," *Appl. Phys. Lett.* **88**, 261103 (2006).
38. V. Blank, M. D. Thomson, and H. G. Roskos, "Spatio-spectral characteristics of ultra-broadband THz emission from two-colour photoexcited gas plasmas and their impact for nonlinear spectroscopy," *New J. Phys.* **15**, 075023 (2013).
39. P. Klarskov, A. C. Strikwerda, K. Iwaszczuk, and P. U. Jepsen, "Experimental three-dimensional beam profiling and modeling of a terahertz beam generated from a two-color air plasma," *New J. Phys.* **15**, 075012 (2013).
40. A. Gorodetsky, A. D. Koulouklidis, M. Massaouti, and S. Tzortzakis, "Physics of the conical broadband terahertz emission from two-color laser-induced plasma filaments," *Phys. Rev. A* **89**, 033838 (2014).